Journal of
Synchrotron Radiation

ISSN 0909-0495

Received 19 September 2005
Accepted 23 November 2005

Radiation driven collapse of protein crystals

Sébastien Boutet‡ and Ian K. Robinson*¶

Department of Physics, University of Illinois, Urbana, IL 61801, USA. E-mail: i.robinson@ucl.ac.uk

During coherent X-ray diffraction measurements on crystals of ferritin at room temperature using monochromatic undulator radiation from the Advanced Photon Source, a sudden lattice contraction was observed following a characteristic latent period and ultimately leading to the collapse of the crystal. The progression of this collapse is analysed using a two-state Hendricks–Teller model. It reveals that 55% of the layers collapse by 1.6% before the crystal completely stops diffracting.

Keywords: radiation damage; proteins; ferritin; coherent X-ray diffraction; lattice contraction.

1. Introduction

Synchrotron X-ray beams have proved since their first use to be extremely useful and powerful tools for studying the structure of matter and even its dynamics (Als-Nielsen & McMorrow, 2001). One might argue that there exists no better tools to study the structure of matter in three dimensions. The high flux of the synchrotron sources have allowed researchers to make great advances in the study of surfaces (Als-Nielsen & McMorrow, 2001; Robinson, 1986) and the study of ever smaller samples. In the case of inorganic materials, the X-ray beam can generally be considered completely non-intrusive as it affects in no way the sample and its properties. This has allowed researchers to use the full potential of the synchrotron beam and its high flux. Unfortunately, this is not true of biological samples. Even though great strides have been made in biological research using synchrotron beams (Fanchon *et al.*, 2000), there is always a limitation on the use one can make of them with biological samples because of sample damage caused by the intense beam.

Many scientists have studied radiation effects on biological samples to various levels of detail (O'Neill *et al.*, 2002; Murray *et al.*, 2004; Nave & Garman, 2005). One can never completely eliminate the problem but many ways have been devised to mitigate it. One such method is the flash-freezing method in which the sample is rapidly cooled to liquid-nitrogen temperature or below before it is put in the X-ray beam. This has the effect of freezing the structure, making it more difficult to damage and to reduce the thermal damage caused by heat generated by the absorption of the X-rays. It also slows down the diffusion of free radicals in the solution which wander around destroying multiple molecules. Another way to reduce the effects of free radicals is to use scavenger molecules in the sample (Murray & Garman, 2002). These scavenger molecules absorb the free radicals that form by ionization in the beam, preventing them from causing further damage.

The process by which biological samples and in particular protein crystals are destroyed in an X-ray beam is not fully understood. We present here some intriguing data that we obtained while performing a coherent X-ray diffraction (CXD) experiment. CXD is a technique which uses the coherence properties of a synchrotron beam to image crystalline nanoparticles in three dimensions (Robinson *et al.*, 2001; Williams *et al.*, 2003). An X-ray beam is considered coherent when the phase of the beam is well defined over the entire sample it illuminates. In this case, every scattered beam from any part of the sample can interfere coherently with any other scattered beam. The result of this is a diffraction pattern which not only yields Bragg peaks from the crystalline lattice but also shows the Fourier transform of the entire particle (Robinson *et al.*, 2001; Williams *et al.*, 2003). One can measure this Fourier transform of the shape of the crystalline particle by carefully measuring the scattering at and around any Bragg peak.

The CXD technique seems ideally suited to the study of protein crystal formation at the early stages when the crystals are too small to be seen with a visible-light microscope. When a supersaturated solution of proteins is prepared, proteins are over time excluded from the solution and they will either precipitate, form amorphous aggregates or, if the conditions are right, form well ordered crystals. The formation of crystals is usually fairly slow and proceeds in two different stages: nucleation and growth (McPherson, 1999).

The nucleation process is ultimately the more interesting one to study with CXD because less is known about it. At all times in solution, proteins form clusters which then redissolve as fluctuations occur. The clusters formed, if large enough that there is an overall lowering of the free energy of the system,

‡ Present address: Stanford Linear Accelerator Center, Stanford University, 2575 Sand Hill Road, Menlo Park, CA 94025, USA. Email: sboutet@slac.stanford.edu.
¶ Present address: Department of Physics and Astronomy, University College, London WC1E 6BT, UK.

will be more likely to keep growing than they are to redissolve. Clusters of that size are called critical nuclei. This size depends on many thermodynamic parameters such as concentration, temperature, pressure and pH and can range from a few molecules at high saturation to infinity for non-saturated solutions (Chernov, 1984; Chernov & Komatsu, 1995).

The critical nuclei form the seeds of the eventual macroscopic protein crystals that one seeks to produce. The growth of these crystals proceeds by successive addition of layers and usually takes from a few hours to days in order to obtain good quality crystals. The growth needs to proceed slowly in order for it to be orderly. This slow growth would make protein crystals ideal for the study of the growth process in real time with X-rays if it were not for the fact that the X-ray beam damages them long before they would have a chance to grow. It has, however, proved possible to study the growth with other techniques such as atomic force microscopy (Yau, Petsev *et al.*, 2000; Yau, Thomas & Vekilov, 2000) which perturbs the process in a different way.

It should be possible, however, to take a snapshot of a small crystal using coherent X-rays, then throw it away and do the same with a different crystal which is at a later state of formation. The same thing could be done at many stages of the crystal growth process to obtain a picture of the evolution in time of protein crystals. Since the exposure time to each sample would be short, radiation damage would be minimized.

This is what we attempted to do using the coherent diffraction method. At present, the technique allows the imaging of crystals of size between 0.1 and a few micrometers. This size range is above the size normally expected for critical nuclei of proteins. However, it is below what can be seen with a light microscope and still within the range of sizes at which protein crystals are typically still in the growth phase. These coherent diffraction experiments on protein crystals can prove difficult due to many experimental obstacles. For example, it can prove difficult to immobilize the crystals sufficiently to allow for a long enough time to collect good data. This problem could be solved with even more brilliant X-ray beams coupled with much faster detectors. However, one problem which cannot be circumvented is associated with the damage caused by the X-ray beam to the crystals. In the process of performing these experiments, catastrophic destruction of the sample was observed, which is the main subject of this paper.

2. Sample and experimental set-up

The protein studied was holoferritin extracted from horse spleen and obtained from Sigma-Aldrich. Its macromolecular assembly is composed of 24 subunits arranged in 432 symmetry forming a roughly spherical shell (inner diameter $\simeq$ 80 Å, outer diameter $\simeq$ 130 Å, MW = 474 kDa). It has the biological function of storing iron in its cavity and releasing it when it is needed by the body (Harrison & Arosio, 1996). The presence of iron greatly increases the signal level and increases the mass of the protein by roughly 50%. It readily crystallizes into the face-centered cubic (f.c.c.) lattice with lattice parameter a = 183 Å when cadmium salt is added. Two Cd^{2+} form salt bridges at every twofold axis of the protein (Granier *et al.*, 1997). Ferritin was obtained at a concentration of 100 mg ml^{-1} in 0.15 *M* NaCl.

The CXD experiments were performed at sector 34-ID-C at the Advanced Photon Source at Argonne National Laboratory. The undulator gap was set so that the fundamental energy was 9 keV. A double Si(111) crystal monochromator was used. The beam was unfocused and slits 1 m upstream of the sample cut the beam down to 200 µm × 200 µm. The samples consisted of a 3 µl drop of 100 mg ml^{-1} ferritin solution placed onto a siliconized glass slide which was glued onto a Peltier cooler. This allowed the temperature to be controlled. The ferritin drop was aligned into the X-ray beam. A 3 µl drop of 60 m*M* $CdCl_2$ was then added to the ferritin drop. This recipe was found to produce a large number of micrometer-sized crystals almost immediately. This large number of crystals is necessary because of the impossibility of orienting the small crystals in a desired way. Instead, one needs to rely on chance by having enough crystals present in solution so that there is a good probability that at least one will meet the Bragg condition and a peak can be observed. A direct-reading CCD camera with pixel size of 20 µm from Roper Scientific was placed 2.2 m away from the sample on the diffractometer detector arm. This arm was then raised to a position where the CCD camera would be at an angle 2θ above the direct beam to meet the Bragg condition for the desired reflection.

As soon as the Cd salt was added to the ferritin solution, the experimental hutch was closed and the beam turned on. It was found that there were already a large number of crystals present, resembling powder diffraction. However, the diffraction rings observed were not continuous and individual Bragg peaks could be seen. Sometimes the peaks overlap too much which indicates that the recipe used produced too many crystals for this experiment to be performed. Ideally one would like to measure just one Bragg peak at a time, so the crystallization recipe used was adjusted to reduce the number of crystals.

3. Results

Fig. 1 shows one frame of a time series of images obtained from a sample containing small ferritin crystals prepared as described above. This frame is a typical example of data obtained on many different occasions. On the image, one can see distinct peaks of intensity lying on two distinct rings. Calibration of the experimental set-up reveals that these rings lie at values of the momentum transfer (q), corresponding to the first two Bragg peaks of f.c.c. ferritin crystals. The momentum transfer is defined as $q = (4\pi/\lambda)\sin\theta$, where λ is the wavelength of the X-rays and θ is the scattering angle. Each of these peaks represents a Bragg peak from a different crystal. From the average number of peaks seen in one image, one can calculate the overall number of crystals present in the sample. The crystals are randomly oriented and the image represents only 25° of the entire powder ring. The rocking curves of the crystals were determined to be roughly 0.3°.

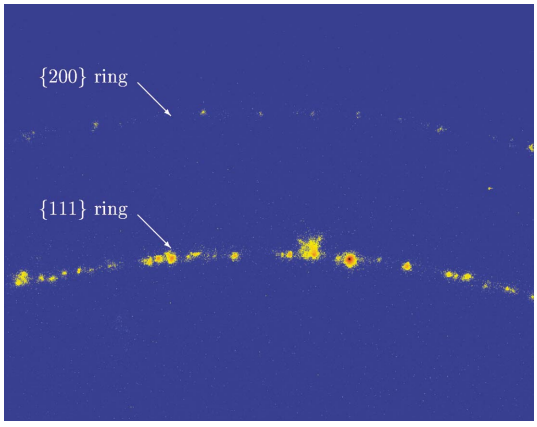

Figure 1
Diffraction from many small ferritin crystals. Individual peaks come from separate crystals. The peaks seen lie on the {111} and {200} rings, the first two rings for f.c.c. crystals. One of the Bragg peaks near the middle of the {111} ring is seen to explode

From this and the fact that a typical image displays 25 Bragg peaks or so, one obtains a total of ∼95000 crystals illuminated by the beam. The size of the beam was 200 μm × 200 μm and the path length inside the sample was 1 mm for a total volume of 0.04 μl. This gives a total of roughly 2.4×10^6 crystals per μl inside the sample. If we assume that all the protein molecules originally in solution have crystallized, we can calculate the average size of the crystals to be ∼5.5 μm × 5.5 μm ×5.5 μm. From the angular width of each Bragg peak, using the Scherrer formula, we can estimate the size of the diffracting crystal to be on average ∼3 μm × 3 μm × 3 μm, which indicates that a large fraction (∼16%) of the proteins are included in crystals.

The position of the peaks as well as their intensity and width change from frame to frame in the time series. There are two main changes observed. The first one is a simple appearance or disappearance of a Bragg peak. The disappearances can be due either to movements of the crystal in solution or to radiation damage, while appearances are due only to motions of the crystals such as diffusion and rotation. The crystals are free to rotate and diffuse in the solution and so a crystal in the Bragg condition which appears as a peak on the CCD can rotate out of the Bragg condition or simply diffuse out of the beam which makes the peak disappear. We know that the crystals are indeed rotating in the solution since we have observed peaks rotate around the Bragg ring which can only occur if the crystal is rotating about the incident beam direction. This is an example of the second kind of changes seen in the diffraction pattern over time, a more gradual change occurring over many images rather than a simple appearance or disappearance of a peak.

After about 30 min of elapsed time, some of those gradual changes observed became quite striking. In many cases a Bragg peak would be stable for a few minutes and then it would gradually expand in reciprocal space in a manner resembling an explosion. The Bragg peak itself would enlarge rapidly and shift toward a larger value of q. We attribute this effect to radiation damage.

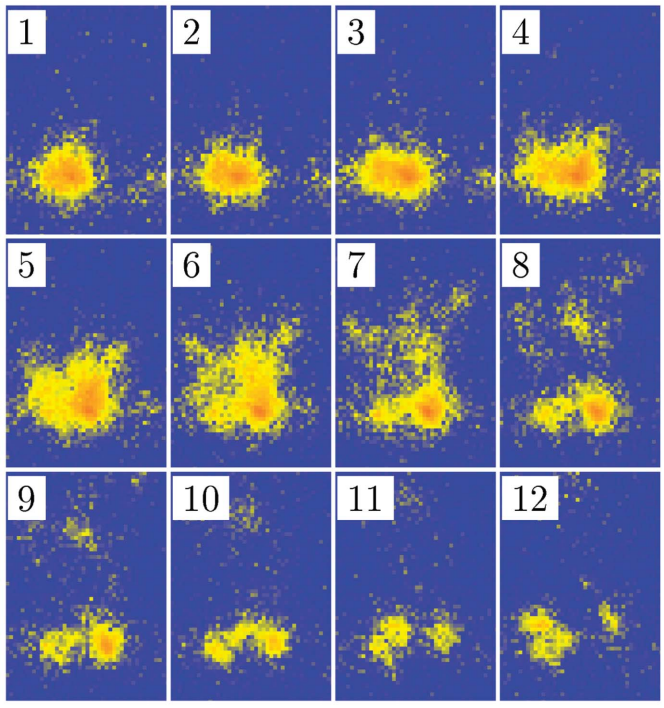

Figure 2
Evolution of a Bragg peak over time. Images of the logarithm of the intensity of a single Bragg peak over time. Each image is taken 95 s apart. After a period where the peak was stable, it breaks up into multiple peaks which move radially to higher q with time.

The effect of radiation on a typical single small crystal of holoferritin is shown in Fig. 2. Adjacent frames of 95 s exposure are shown starting 19 min from the start of irradiation. The image of the Bragg peak is seen to be stable for the first 25 min before breaking into a complicated distribution with multiple peaks. As time goes by, these peaks are seen to move up on the image, which in this particular case corresponds to a higher value of q. The origin in reciprocal space was located below the image, and the movement of the intensity toward higher q was radial.

Many similar Bragg peak explosions have been observed with different samples. In all cases, the Bragg peak was seen to be stable for a latent period varying between 10 and 30 min before the peak started to change. The intensity of a few of these exploding Bragg peaks was integrated radially and turned into an intensity curve *versus* q. This is shown in Fig. 3 for a (111) Bragg peak and in Fig. 4 for a (200) Bragg peak.

Fig. 3 is the integrated data from Fig. 2 and is a typical example of a Bragg peak which was seen from the start of the measurement. The peak eventually breaks up into many parts. One part remains at the original q value of the ferritin crystal while other parts slowly move to higher q with time.

In some cases the Bragg peak did not break up into many distinguishable parts and it was stable for a period of time before the entire intensity shifted to a higher value of q. This is shown in Fig. 4 for a (200) peak. Compared with Fig. 3, the entire crystal now undergoes changes with time and not just parts of it.

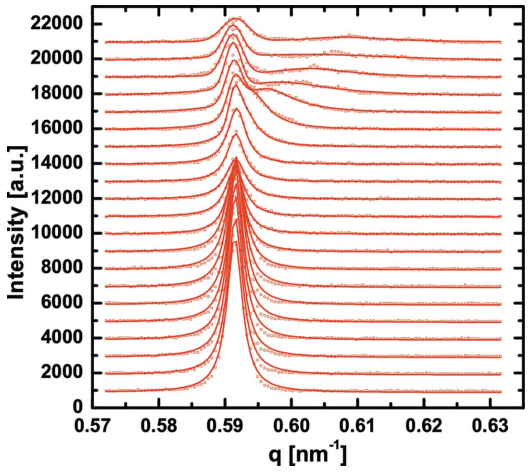

Figure 3
Radial intensity distribution from a (111) Bragg peak *versus* time. Each curve corresponds to a different time moving from the bottom curve to the top curve in increments of 95 s. The circles represent the azimuthally integrated intensity data with the solid curve corresponding to a fit using a simple Hendricks–Teller model.

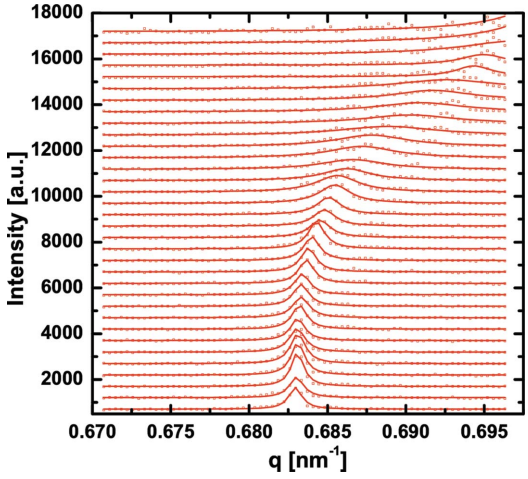

Figure 4
Radial intensity distribution from a (200) Bragg peak *versus* time. Each curve corresponds to a different time moving from the bottom curve to the top curve in increments of 95 s. The circles represent the azimuthally integrated intensity data with the solid curve corresponding to a fit using a simple Hendricks–Teller model.

A change in the q position of a peak represents a change in the lattice spacing of the crystal. Such changes in lattice spacing have been observed before for protein crystals and in particular ferritin crystals (Ravelli *et al.*, 2002). These authors showed that the lattice of ferritin crystals tends to expand when exposed to X-rays. However, all of these measurements were performed at temperatures between 80 K and 180 K while our measurements were all carried out at room temperature.

While changes in lattice spacing are not surprising with radiation exposure, what is very surprising about the results shown in Figs. 3 and 4 is that we observe a change towards higher q, which corresponds to a smaller spacing in real space. The observation of contraction rather than expansion is contrary to what most studies on the effect of radiation on the lattice spacing of protein crystals have revealed (Murray & Garman, 2002; Ravelli *et al.*, 2002). However, some cases of contraction with radiation dose have been published by Ravelli *et al.* (2002). While most of their results indicate an expansion of the lattice with dose, all of these were at low temperature. The highest temperature measurement they reported was at 180 K and this single measurement actually showed a lattice contraction.

Radiation damage to protein crystals has been shown to be dependent on accumulated dose and not dose rate (Nave & Garman, 2005). We therefore calculated the dose absorbed by the small crystals per second. The density of the ferrihydrite in the iron core is roughly half the density of iron. Using that fact, we can calculate the X-ray absorption coefficient of the iron core. We also calculate the absorption coefficient of the water in the crystal as well as the protein shell itself. We obtain a total absorption coefficient μ and calculate the fraction of X-rays hitting the sample that are absorbed,

$$\text{Abs} = 1 - \exp(-\mu l), \tag{1}$$

where $l = 3$ µm is the path length inside the crystal. This path length was estimated from the width of the Bragg peak using the Scherrer formula. At 9 keV, most of the absorption is due to the iron and so, while the iron gives an enhancement in intensity which is needed to perform CXD measurements, it simultaneously increases the damage limiting the applicability of the technique. We find that ~8% of the X-rays hitting a typical crystal are absorbed by it.

The number of X-rays hitting the crystal per second can be obtained using the measured current in the ion chamber beam monitor. For a beam of 25 µm × 25 µm at 9 keV, the measured flux is 1.64×10^8 photons s^{-1}. Therefore the flux hitting a 3 µm × 3 µm crystal is 2.37×10^6 photons s^{-1}. The standard unit of dose is the Gray (Gy = J kg^{-1}). The energy deposited per photon is just the energy of the photon, which was 9 keV. We then have 3.4×10^{-9} J s^{-1} crossing the surface of the crystal. We know the mass of the protein (~725 kDa when fully loaded with iron) and the structure of the crystal and we can then calculate the total mass of the crystal and obtain 2.1×10^{-14} kg. The absorbed dose in Gy s^{-1} is then

$$\begin{aligned}\text{Dose rate} &= \text{Abs} \times 3.4 \times 10^{-9}\,[\text{J s}^{-1}] \times \frac{1}{2.1 \times 10^{-14}\,[\text{kg}]} \\ &= 1.3 \times 10^4\,\text{Gy s}^{-1}.\end{aligned} \tag{2}$$

This is our conversion factor from time to dose. This number is only an approximation since we do not know the exact size of the crystal. Henderson has shown that the dose limit where half of the intensity is lost for protein crystals at cryogenic temperature is 2×10^7 Gy (Henderson, 1990). The limit is significantly lower by a factor of 70 for room temperature (Nave & Garman, 2005). Nevertheless, with such a dose rate we expect to reach the Henderson limit in roughly 30 min. In the present case, a dose of 2×10^7 Gy corresponds to an average of roughly 15 absorption events per protein molecule in the crystal.

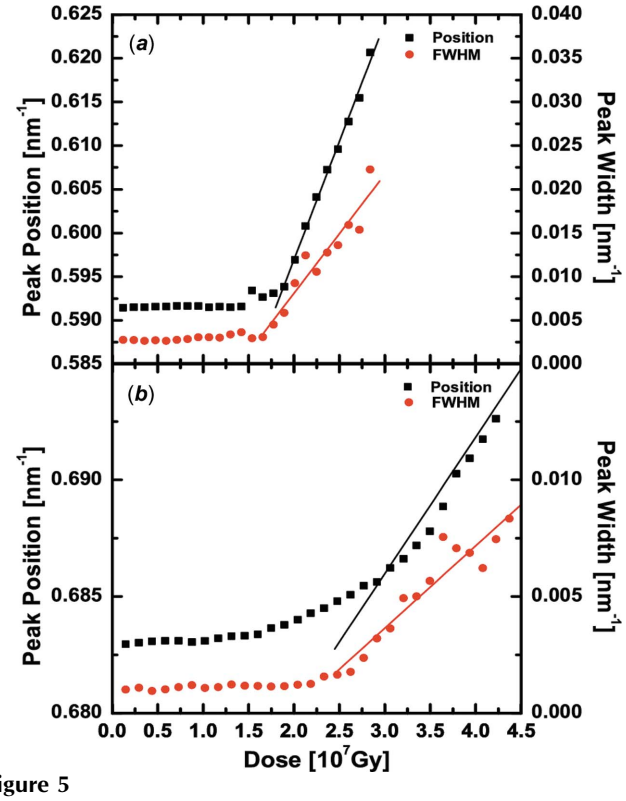

Figure 5
Position and width of (*a*) the (111) Bragg peak shown in Fig. 3 and (*b*) the (200) Bragg peak shown in Fig. 4 *versus* dose. There is a stable latent period followed by a roughly linear in time increase with dose of both parameters. The peaks were fitted to a Gaussian to extract the q position and the width.

To quantify the lattice spacing change with dose, each curve was fitted to a Gaussian and the position of the peak was extracted as well as its width. The two quantities are plotted *versus* dose in Fig. 5(*a*) for a (111) peak and in Fig. 5(*b*) for a (200) peak. In both cases shown, and many others investigated, there is a latent period where there is no change in the lattice spacing and the width of the peak. After a certain time or dose, which varies from crystal to crystal, there is a roughly linear increase in both the position and the width of the peak.

The data shown are surprising, but clearly represent a collapse of the crystals with increasing dose. The gradual change *versus* dose suggests a cumulative process. To attempt to understand the behavior we consider that, over time and with increasing dose, some specific and non-specific damage occurs to individual proteins in the crystal. The radiation presumably causes some point defects randomly distributed in the crystal by destroying parts of the protein molecule. The direct interaction between an X-ray photon and an electron in the crystal produces a free radical and this is known as primary damage. Primary damage will likely, at first, change slightly the quaternary structure of the molecule and therefore change how it interacts with neighbor molecules. Secondary damage also occurs from a cascade of radicals formed by the propagation of the original radical created (Murray & Garman, 2002). It is known that a crystal can accommodate a limited density of point defects while maintaining its long-range order and therefore a crystal can withstand some small changes in the structure of some of the proteins without any visible adverse effects. However, after a certain dose, the defects in the crystal apparently reach a critical density beyond which the crystal is no longer stable and it undergoes an amorphization transition. Some parts of it therefore reorganize into a more stable structure. In our case, the evidence indicates that these defects are contractions in the spacing of the crystal layer. Once these defects start to occur, their number keeps increasing. It is known that long wavelength fluctuations in two dimensions cause the displacement from the lattice sites to diverge logarithmically with crystal size, according to the Mermin–Wagner theorem (Mermin, 1968; Mermin & Wagner, 1966). A crystal with sufficient defects eventually just undergoes a transition to what must be described as an amorphous structure. The question of how many defects a crystal can have and maintain its lattice is generally unanswered. The value of 10% is often used as a rough estimate. Models such as the Kinchin–Pease model have been developed to calculate the effect of radiation on the structure of inorganic crystals (Kinchin & Pease, 1955). Such a model is difficult to use for protein crystals owing to the difficulty in determining the effect of radiation on the protein. The X-ray photon does not simply knock a protein molecule out of the lattice creating a vacancy. The details of the interaction and defect formation are not well understood.

In order to make this a little more quantitative, we performed an analysis of the data using a Hendricks–Teller-type model (Hendricks & Teller, 1942). Such a model is often used to study the diffraction from crystals with a varying number of random defects with a size mismatch to the host (Robinson *et al.*, 1996). The exact model, in one dimension, applies to a linear array of objects spaced apart by distances L_j chosen at random with probability f_j. The diffracted intensity from a crystal with defects is thus modeled as a regular spacing L_0 with randomly inserted defects of spacings L_j of probability f_j. The intensity is given by the following expression,

$$I(q) = \frac{1 - C^2}{1 - 2C\cos\varphi + C^2}, \tag{3}$$

where

$$C = \sum_j f_j \cos\left(qL_j + \varphi\right) \tag{4}$$

and φ is an average crystallographic phase factor given by

$$\tan\varphi = \sum_j f_j \sin(qL_j) \Big/ \sum_j f_j \cos(qL_j). \tag{5}$$

f_j is the probability that a spacing of length L_j will occur. To apply a one-dimensional model in our case means that the elementary defects modeled are planes of modified thickness.

In our case we used the simplest model possible with only one type of defect with a spacing different from the expected crystal spacing. The intensity profile was then completely determined by performing a fit of the data with only two free parameters: a spacing L_1 and a probability f_1 in a host of known spacing L_0 with probability $f_0 = 1 - f_1$. Each curve shown as a solid line in Figs. 3 and 4 are the fits to the data

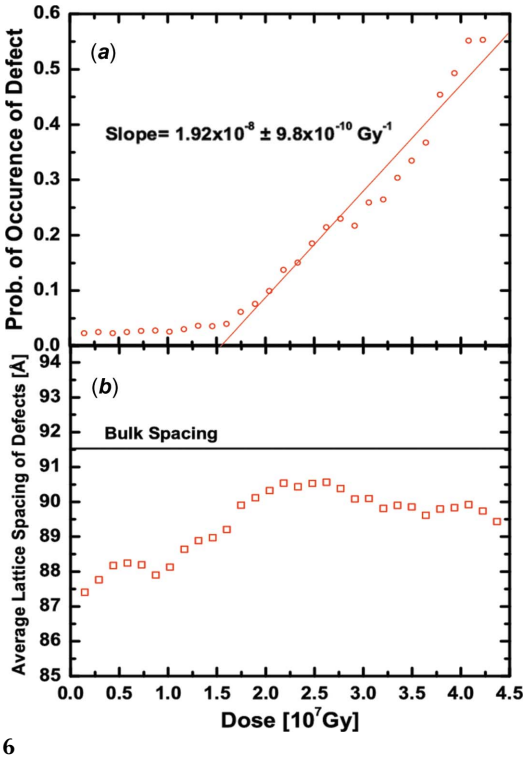

Figure 6
(*a*) Probability of occurrence of a radiation-induced defect in the crystal obtained by fitting a Hendricks–Teller model to the time evolution of a (200) Bragg peak. After a latent period, the probability increases linearly with time. (*b*) Fitted value of the spacing of the radiation-induced defects in the crystal. The values obtained for the spacing during the latent period are unreliable. Once the crystal starts to disintegrate, the fitted value is fairly constant (90 Å) and is about 2 Å below the indicated bulk value for a defect-free crystal (91.5 Å).

using this Hendricks–Teller two-state model with, in the case of Fig. 3, a Gaussian to fit the undisplaced peak. The two fitted parameters, a probability for the defects with a lattice spacing of the defect, are shown in Fig. 6 for the (200) Bragg peak.

The probability of occurrence of defects turns out to be essentially zero during the latent period, indicating that even though there has to be damage to individual proteins the damage is small enough not to cause any change in the crystal structure. At the end of this latent period, the Bragg peak position starts to change and a non-zero value of the probability of defects is fitted. A large number of individual point defects on separated protein sites combine to cause a structural change to the crystal. A layer of the crystal collapses to a distance a little closer than normal. Over time, as the absorbed dose increases, more of these defects occur and many more layer spacings collapse to values smaller than the f.c.c. crystal spacing. Eventually, a probability of 0.55 is reached before there is no diffracted intensity measured, which means that the crystal diffracts until 55% of the layers have collapsed.

The fitted values of the spacing seen in Fig. 6(*b*) are unreliable during the latent period because the probability is essentially zero. A defect of any size which has a zero probability of occurrence will give the same diffracted intensity as any other defect with a zero probability. This latent period is seen to last until a dose of roughly 1.5×10^7 Gy is absorbed. After that point the spacing fitted can be trusted and it is seen to fluctuate slightly around a value of 90 Å. This value was allowed to vary freely because we have no reason to expect a particular new spacing to occur.

The process by which this new spacing is created is a highly uncontrolled destructive process which we have no means of predicting. The perfect crystal spacing for the (200) Bragg peak of f.c.c. ferritin is 91.5 Å. This means that individual layers of the crystal collapse by 1.5 Å or 1.6%. This is fairly large considering the fact that the f.c.c. crystal of ferritin is close-packed and the distance should not be allowed to contract. The contacts between proteins are along the face-diagonal of the crystal and mediated by two Cd^{2+} salt bridges. There is essentially no room between the proteins along the face-diagonal with the insertion of these salt bridges. In order for the (200) lattice spacing to collapse, which corresponds to the edges of the cubic unit cell, one mechanism might be entire removal of the salt bridges, which each occupy roughly 3 Å. The damage from the X-rays must cause these links to be destroyed, most likely by destroying the residues involved in the contact. However, that fact alone does not explain why the crystal collapses.

The removal of the salt bridges could just as well cause the proteins to move apart rather than move closer together. Water could fill the empty space between the proteins and cause them to move apart. There must then also be a removal of the interstitial water near the protein contacts allowing the observed collapse. This could be due to a heating effect from the intense X-ray beam causing the interstitial water to diffuse away. Solvent boiling is, however, unlikely considering that the sample is mounted on a large heat sink which means that very slow heating of the sample cannot occur. It is conceivable that rapid heating could occur for a small volume on timescales shorter than the time it takes for the heat to be conducted away. However, the whole process occurs over tens of minutes which is more than enough time for the heat sink to cool any hot spot in the sample.

Numerical simulations by Mhaisekar *et al.* have shown that beam heating is not a significant factor at cryogenic temperatures (Mhaisekar *et al.*, 2005). Whether this is also the case at room temperature is unclear. Also, it is a well known fact that X-ray radiation damage is a dose-related problem (Nave & Garman, 2005), which indicates that the main factor is not boiling of the solvent.

Intentional dehydration of protein crystals is often carried out as part of the post-crystallization treatment in order to try to improve the diffraction of the crystal (Heras & Martin, 2005). Dehydration of the crystal generally leads to a shrinkage of the lattice spacing. The collapse of the crystals described in this paper may very likely involve dehydration. It is, however, unclear how this occurs.

4. Conclusion

Our data are low-resolution data which does not allow us to make any specific claims as to the atomic level mechanism involved in the destruction of the crystal. Since we only

measure the first orders of Bragg peaks, we are fairly insensitive to small changes in the position of individual atoms caused by the beam. It is well known that the higher-order reflections disappear first during data collection on a protein crystal. By the time we measure a significant change in the (200) peak, the crystal should have long stopped diffracting at higher q. Our investigation examines the stability of the crystal lattice rather than the specific changes in individual molecules. Spot fading studies, sensitive to the latter effect, find changes at high q at lower doses than what we see (Murray & Garman, 2002; Ravelli *et al.*, 2002). However, the measured onset of the linear changes in the lattice with dose matches well with the Henderson limit. This is surprising because the limit is reported to be 70 times lower at room temperature (Nave & Garman, 2005), where our measurements were made. There is speculation that very small protein crystals near 1 μm in size would be less sensitive to radiation than larger crystals since the photoelectrons created by the interaction of the X-rays with matter would be able to escape the small crystal before creating a lot of damage (Nave & Hill, 2005). Our results could be an indication of that. However, we cannot tell what is happening to the higher diffraction orders and cannot conclude about the spot fading of these peaks.

Although no specific crystal interactions can be inferred from our data, we can still learn some interesting facts about the late stage of radiation damage on protein crystals, especially small crystals only a few micrometers in size. The entire crystal is illuminated by the X-ray beam and the measurements are averaged over the entire crystal. It is interesting to note that the crystal can survive with as much as 55% defects in the lattice spacing. Also, the crystals seem to break up into many separate blocks which all have slightly different lattice spacings and each of which is stable for a significant amount of time, as much as 5 min.

This research was supported by the NSF under grants DMR03-08660. The UNICAT facility at the Advanced Photon Source is supported by the University of Illinois at Urbana-Champaign, Materials Research Laboratory (US DOE contract DEFG02-91ER45439, the State of Illinois-IBHE-HECA, and the NSF), the Oak Ridge National Laboratory (US DOE under contract with UT-Battelle LLC), and the National Institute of Standards and Technology (US Department of Commerce). One of the authors (SB) wishes to thank the 'Fonds québécois de la recherche sur la nature et les technologies' for its support.

References

Als-Nielsen, J. & McMorrow, D. (2001). *Elements of Modern X-ray Physics*. New York: Wiley.
Chernov, A. (1984). *Modern Crystallography III: Crystal Growth*. Berlin: Springer-Verlag.
Chernov, A. & Komatsu, H. (1995). *Principles of Crystal Growth in Protein Crystallization*. Dordrecht: Kluwer.
Fanchon, E., Geissler, E., Hodeau, J.-L., Regnard, J.-R. & Timmins, P. A. (2000). *Structure and Dynamics of Biomolecules: Neutron and Synchrotron Radiation for Condensed Matter Studies*. Oxford University Press.
Granier, T., Gallois, B., Dautant, A., Destaintot, B. & Precigoux, G. (1997). *Acta Cryst.* D**53**, 580–587.
Harrison, P. M. & Arosio, P. (1996). *Biochim. Biophys. Acta*, **1275**, 161–203.
Henderson, R. (1990). *Proc. R. Soc. London Ser. B*, **241**, 6–8.
Hendricks, S. & Teller, E. (1942). *J. Chem. Phys.* **10**, 147.
Heras, B. & Martin, J. (2005). *Acta Cryst.* D**61**, 1173–1180.
Kinchin, G. & Pease, R. (1955). *Rep. Prog. Phys.* **18**, 1–51.
McPherson, A. (1999). *Crystallization of Biological Macromolecules*. Cold Spring Harbor Press.
Mermin, N. (1968). *Phys. Rev.* **176**, 250–254.
Mermin, N. & Wagner, H. (1966). *Phys. Rev. Lett.* **17**, 1133–1136.
Mhaisekar, A., Kazmierczak, M. & Banerjee, R. (2005). *J. Synchrotron Rad.* **12**, 318–328.
Murray, J. & Garman, E. (2002). *J. Synchrotron Rad.* **9**, 347–354.
Murray, J., Garman, E. & Ravelli, R. (2004). *J. Appl. Cryst.* **37**, 513–522.
Nave, C. & Garman, E. F. (2005). *J. Synchrotron Rad.* **12**, 257–260.
Nave, C. & Hill, M. (2005). *J. Synchrotron Rad.* **12**, 299–303.
O'Neill, P., Stevens, D. & Garman, E. (2002). *J. Synchrotron Rad.* **9**, 329–332.
Ravelli, R., Theveneau, P., McSweeney, S. & Caffrey, M. (2002). *J. Synchrotron Rad.* **9**, 355–360.
Robinson, I., Eng, P., Romainczyk, C. & Kern, K. (1996). *Surf. Sci.* **1367**, 105–112.
Robinson, I. K. (1986). *Phys. Rev. B*, **33**, 3830–3836.
Robinson, I., Vartanyants, I., Williams, G., Pfeifer, M. & Pitney, J. (2001). *Phys. Rev. Lett.* **87**, 195505.
Williams, G., Pfeifer, M., Vartanyants, I. & Robinson, I. (2003). *Phys. Rev. Lett.* **90**, 175501.
Yau, S.-T., Petsev, D., Thomas, B. & Vekilov, P. G. (2000). *J. Mol. Biol.* **303**, 667–678.
Yau, S.-T., Thomas, B. & Vekilov, P. G. (2000). *Phys. Rev. Lett.* **85**, 353–356.